Journal of Environmental Management 187 (2017) 229–238

Contents lists available at ScienceDirect

Journal of Environmental Management

journal homepage: www.elsevier.com/locate/jenvman

Research article

Uncertainties in mapping forest carbon in urban ecosystems

Gang Chen [a, *], Emre Ozelkan [a, b], Kunwar K. Singh [c, d], Jun Zhou [e], Marilyn R. Brown [a], Ross K. Meentemeyer [c, d]

[a] Laboratory for Remote Sensing and Environmental Change (LRSEC), Department of Geography and Earth Sciences, University of North Carolina at Charlotte, Charlotte, NC 28223, USA
[b] Agricultural & Environmental Informatics Research and Application Centre, Istanbul Technical University, Istanbul, Turkey
[c] Center for Geospatial Analytics, North Carolina State University, Raleigh, NC 27695, USA
[d] Department of Forestry and Environmental Resources, North Carolina State University, Raleigh, NC 27695, USA
[e] Department of Urban Planning, School of Urban Design, Wuhan University, Wuhan, Hubei 430072, China

ARTICLE INFO

Article history:
Received 27 March 2016
Received in revised form
15 September 2016
Accepted 25 November 2016

Keywords:
Urban forest
Carbon mapping
Uncertainty analysis
Remote sensing resolution
Neighborhood pattern

ABSTRACT

Spatially explicit urban forest carbon estimation provides a baseline map for understanding the variation in forest vertical structure, informing sustainable forest management and urban planning. While high-resolution remote sensing has proven promising for carbon mapping in highly fragmented urban landscapes, data cost and availability are the major obstacle prohibiting accurate, consistent, and repeated measurement of forest carbon pools in cities. This study aims to evaluate the uncertainties of forest carbon estimation in response to the combined impacts of remote sensing data resolution and neighborhood spatial patterns in Charlotte, North Carolina. The remote sensing data for carbon mapping were resampled to a range of resolutions, i.e., LiDAR point cloud density – 5.8, 4.6, 2.3, and 1.2 pt s/m^2, aerial optical NAIP (National Agricultural Imagery Program) imagery – 1, 5, 10, and 20 m. Urban spatial patterns were extracted to represent area, shape complexity, dispersion/interspersion, diversity, and connectivity of landscape patches across the residential neighborhoods with built-up densities from low, medium-low, medium-high, to high. Through statistical analyses, we found that changing remote sensing data resolution introduced noticeable uncertainties (variation) in forest carbon estimation at the neighborhood level. Higher uncertainties were caused by the change of LiDAR point density (causing 8.7–11.0% of variation) than changing NAIP image resolution (causing 6.2–8.6% of variation). For both LiDAR and NAIP, urban neighborhoods with a higher degree of anthropogenic disturbance unveiled a higher level of uncertainty in carbon mapping. However, LiDAR-based results were more likely to be affected by landscape patch connectivity, and the NAIP-based estimation was found to be significantly influenced by the complexity of patch shape.

1. Introduction

Urban forests can provide a myriad of ecosystem services, such as air pollution reduction, biodiversity preservation, climate amelioration, water quality improvement, and leisure enhancement to improve public health and human development (Dwyer et al., 1992; Wear et al., 1998; Tyrväinen and Miettinen, 2000; Alvey, 2006; Nowak et al., 2013). In North America, municipal governments play a vital role in protecting, planting, and maintaining trees that grow on public lands (e.g., street and park trees). A number of cities have developed urban forest management plans (e.g., Charlotte, Seattle, Baltimore, and NYC) to address the growing challenge of declining forest health and extent due to rapid urban development (City of Baltimore 2007; City of Seattle, 2013; City of New York 2014). However, the majority of urban trees actually grow on private lands with limited site accessibility. City managers are facing a common challenge that a municipal-scale forest conservation plan needs to be developed using forest inventories that are biased to street and park trees (Clark et al., 1997).

Remote sensing offers an ideal tool to provide spatially explicit characterization of urban forest with minimum field efforts to address this challenge. Recently, the advances in sensor technology allow the practitioners to retrieve both the forest horizontal structures (e.g., canopy cover – the horizontal extent of canopies

* Corresponding author.
E-mail address: gang.chen@uncc.edu (G. Chen).

http://dx.doi.org/10.1016/j.jenvman.2016.11.062
0301-4797/

per unit land area) and vertical structures (e.g., tree height and carbon storage). Although canopy cover has been a popular parameter to imply the effectiveness of forest management, carbon storage is drawing increasing attention, because it can describe tree growth (e.g., old *versus* young, healthy *versus* damaged) in a more accurate way (Singh et al., 2015a,b). Knowing how much carbon is stored by urban forest can further assists in developing effective climate change mitigation efforts, such as supplying marketable carbon emission offsets in a carbon trading program (Poudyal et al., 2010).

The nature of fragmented development in an urban setting often leads to small, isolated tree patches surrounded by abiotic components. Therefore, high-spatial resolution (hereafter *h-res*) remote sensing data is particularly beneficial for urban forest management. Forest carbon estimation requires accurate answers to two questions: where are the trees? And how much carbon is stored in the spotted trees? The first question can be well addressed by h-res optical sensors, because they have the capacity to differentiate complex land cover types (e.g., forest *versus* building) based on the distinct spectral, spatial, and/or temporal characteristics of fine-scale ground objects (Blaschke et al., 2014). Once trees are located, structural data such as small footprint LiDAR point clouds are ideal to extract plant vertical structure, including understory vegetation (Shrestha and Wynne, 2012; Singh et al., 2015b).

While theoretically promising, applying h-res remote sensing to map forest carbon storage at the municipal scale is often restrained by limited budget, as the costs associated with h-res data acquisition and processing remain high. A potential solution is to use coarser-resolution data. But, can such data still generate satisfactory results meeting the needs of urban forest management? Previous efforts exploring the resolution-accuracy relationship mainly focused on natural forests (e.g., Treitz et al., 2012; Jakubowski et al., 2013). However, studying the similar topic in an urban setting has received less attention (Singh et al., 2015a). This is because urban environments are highly fragmented where neighborhoods vary by levels of forest fragmentation. It is likely that the neighborhood development patterns (e.g., low *versus* high built-up density) further complicate the resolution-accuracy relationship in an urban setting.

To inform effective urban forest management while reducing costs, this study aims to improve our understanding of the uncertainties in urban forest carbon mapping through assessing the joint impacts of remote sensing data resolution and neighborhood patterns. We integrated h-res remote sensing data from aerial photography and airborne LiDAR to estimate spatially explicit forest carbon distributions across the Charlotte metropolitan area of North Carolina, United States. The variation in carbon estimation was generated using multiple resolutions of data from aerial imagery and LiDAR point clouds, respectively. We further applied statistical modeling to quantify how such data resolution-induced variation was affected by urban spatial patterns at the neighborhood level.

2. Study area

Our study area covered the entire Charlotte–Mecklenburg County (CMC) of North Carolina, United States, with a size of 1415 km^2 centered at 35°15′N, 80°50′W (Fig. 1). Charlotte, the largest city in North Carolina, has earned the title of “The City of Trees”, and is recognized as one of the “10 best cities for urban forests” by American Forests, the oldest national non-profit citizen conservation organization (American Forests, 2014). Forested landscapes of Charlotte are primarily comprised of secondary growth oak-hickory-pine trees (BenDor et al., 2014). According to the most recent city-maintained forest inventory, approximately 86% of all street trees (~180,000) in Charlotte are deciduous trees with 39% being large maturing species (trees that will grow >40') (City of Charlotte (2013)). Five dominant species, including crape myrtle (*Lagerstroemia* spp.), willow oak (*Quercus phellos*), red maple (*Acer rubrum*), callery pear (*Pyrus calleryana*), and dogwood (*Cornus florida*), represent 50% of the total street tree population, while the remainder is comprised of sugar maple (*Acer saccharum* Marsh.), sweetgum (*Liquidambar*), eastern redcedar (*Juniperus virginiana*), and pear (*Pyrus* spp.) (City of Charlotte (2013)). The trees on private lands, however, still lack detailed inventories compared to the street trees.

Since the mid-1980s, the Charlotte metropolitan area has become one of the fastest developing regions of the southeastern United States. According to U.S. Census Bureau (2015), CMC has grown in population from 0.4 million in 1980 to over 1 million people in 2014, a trend that is expected to continue. The rapid population growth, manifested by an urban geography of low, medium to high housing density, has replaced landscapes dominated by native forest and farmland with an array of developed land use types including managed treescapes and highly fragmented urban forests (BenDor et al., 2014).

3. Data

3.1. Field data

Field mensuration was conducted during 2010–2012 as part of the Charlotte ULTRA-Ex (Urban Long-Term Research Areas Exploratory) study designed to analyze socio-ecological interactions driving the persistence of private forest (Singh et al., 2015b). This research selected a total of 56 circular plots (0.04 ha each) across deciduous (25 plots) and coniferous (21 plots) forests. Those field plots were designed to cover a variety of major species types in the study area, such as Shagbark Hickory (*Carya ovata*), Sweet Gum (*Liquidambar styraciflua*), White Oak (*Quercus alba*), Tulip Poplar (*Liriodendron tulipifera*), Winged Elm (*Ulmus alata*), Willow Oak (*Quercus phellos*), Loblolly Pine (*Pinus taeda*), Mockernut Hickory (*Carya tomentosa*), Pignut Hickory (*Carya glabra*), Tulip Poplar (*Liriodendron tulipifera*), Red Maple (*Acer rubrum*), Short Leaf Pine (*Pinus echinata*), and Eastern Red Cedar (*Juniperus virginiana*). Within each plot, we measured geographic coordinate, tree diameter at the breast height (DBH), species composition, and merchantable tree height. If a plot consisted of over 75% deciduous or coniferous trees, we labeled the plot as deciduous or coniferous, respectively otherwise we labeled plots as mixed plots. We applied the classic Jenkins allometric equations (Jenkins et al., 2003) to calculate forest aboveground biomass (AGB) for all the field plots by following Godwin et al. (2015). Although we recognized that Jenkins equations were developed and complied for a larger areal extent of contiguous United States, the results were considered ‘ground truth’ due to the lack of local equations. McPherson et al. (2013) also argued that such errors are smaller than the high variation in tree growth in urban environments.

3.2. Remote sensing data

Two types of remote sensing data were utilized in this project, including LiDAR point clouds, and NAIP (National Agriculture Imagery Program) multispectral imagery. LiDAR data were acquired by the Storm Water Services Division of Charlotte-Mecklenburg County government office in April 2012, as part a long-term flooding monitoring project. Original data acquisition was carried out using Optech's ALTM Gemini 3100 LiDAR system (Optech Incorporated, Vaughan, Canada), at point densities of 1.0 pts/m^2 for the entire region and 5.8 pts/m^2 for forest-covered areas. We used a

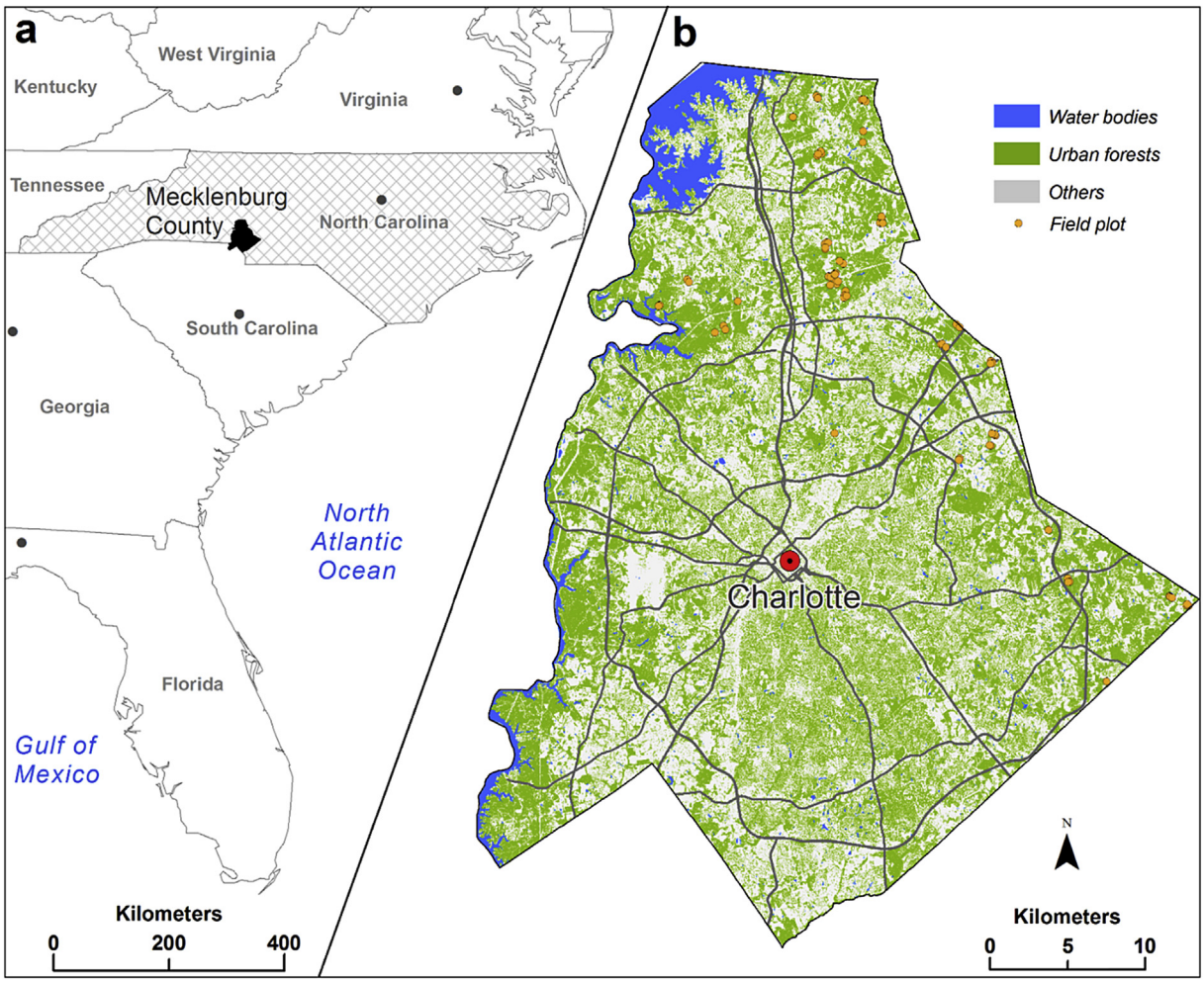

Fig. 1. Study area of the Charlotte-Mecklenburg Country of North Carolina, USA.

total of 1896 tiles (914.4 × 914.4 m each) of LiDAR point clouds. A NAIP image mosaic covering the study area was downloaded from the U.S. Department of Agriculture Geospatial Data Gateway (http://datagateway.nrcs.usda.gov/). The raw images were taken during the leaf-on season in 2012 at 1.0 m spatial resolution with four spectral bands (blue, range of wavelength: 400–580 nm; green, range of wavelength: 500–650 nm; red, range of wavelength: 590–675 nm; and near infrared, range of wavelength: 675–850 nm). The images were geometrically and radiometrically corrected, orthorectified, and mosaicked before being made available online (U.S. Department of Agriculture, 2015).

3.3. Residential neighborhoods

The Charlotte-Mecklenburg Quality of Life Project defined a total of 464 Neighborhood Profile Areas (NPA) in the region (City of Charlotte and Mecklenburg County, 2012). Each NPA represents one or more homogenous census block groups with similar development patterns. We randomly selected 50 NPAs for the succeeding analyses, with a purpose to mitigate the negative impact of spatial autocorrelation among NPAs. Since urban residential neighborhoods vary in development, we adjusted the random selection criterion to include comparative numbers of neighborhoods with built-up densities (i.e., percent built-up: PBU) from low (PBU $\leq$ 15%), medium-low (15% < PBU $\leq$ 25%), medium-high (25% < PBU $\leq$ 40%) to high (PBU > 40%). This approach of neighborhood categorization has proven effective to analyze Charlotte's forest-neighborhood relationship in a previous study by Godwin et al. (2015).

4. Methods

4.1. Urban land-cover mapping

The four-band NAIP image mosaic was employed to extract the wall-to-wall forest canopy cover in the study area. Here, we resampled the image from 1 m to three coarser spatial resolutions 5, 10 and 20 m, with the main purpose to examine the impact of image resolution on canopy cover and carbon storage estimation. The coarsest resolution was chosen to be consistent with the size of field plots. The main purpose of choosing those resolutions was based on our consideration that high-resolution remote sensing should provide equivalent or higher-resolution measurements than those collected from the field. There are normally two typical land-cover image classification schemes: pixel-based *versus* object-based. For the images with resolutions of 1 and 5 m, we selected the object-based scheme, while the pixel-based scheme was utilized to classify the images with coarser resolutions of 10 and 20 m. This was based on two considerations. First, at the high resolutions of 1 and 5 m, individual pixels often represented part of a tree. The variation in leaf reflection angle caused by various species types and the coexistence of sunlit and shaded canopies caused high

spectral 'noises' in classification. The object-based approach grouped neighboring pixels together to create image-objects as the basic study units, which indicated proven success to reduce such noises in forests (Chen et al., 2012). However, at the resolutions 10 and 20 m, the sizes of pixels were often equivalent or larger than the sizes of individual trees in our study area, making it more reasonable to take the classic pixel-based approach. Second, we have compared the performance of both classification schemes at all chosen resolutions with results confirming our assumptions made in the first consideration.

We performed classification in the eCognition Developer 8 environment (Trimble Navigation, California, USA) using four steps: (i) image-objects, representing small tree clusters or individual tree crowns, were generated by the multiresolution segmentation algorithm. The scale parameter of 30 was found to work well for both resolutions of 1 and 5 m. No objects needed to be generated for the pixel-based classification, with the chessboard algorithm used to retain pixels. (ii) The input variables/features for classification included the four NAIP multispectral bands and the corresponding four spectral variation (i.e., standard deviation) bands. (iii) The classic nearest neighborhood classification algorithm was applied to classify all the pixels into six land-cover classes, including deciduous forest (C1), coniferous forest (C2), built-up (C3), open space (C4), water (C5), and bare soil (C6). Here, we categorized forests into two classes, because deciduous and coniferous trees have different forms and their carbon storage is often modeled separately. For each resolution of image, a total of 300 training samples were randomly selected across all image-objects or pixels. Identification of land-cover classes was made through manual photo interpretation and field visits. (iv) The accuracies of results were reported using confusion matrices and kappa statistic. Similar to the extraction of training samples, 300 validation samples were selected following a random selection manner.

4.2. Spatially explicit forest carbon estimation

Estimating forest carbon storage was conducted in two main steps: (i) plot-level carbon modeling with LiDAR and field data; and (ii) application of the plot-level models to estimate spatially explicit carbon storage with LiDAR and NAIP classification maps (Section 4.1). Specifically, (i) LiDAR point clouds were resampled to 100% (no resampling, 5.8 pts/m^2), 80% (4.6 pts/m^2), 40% (2.3 pts/m^2), and 20% (1.2 pts/m^2) for the purpose of analyzing the impact of LiDAR point density on forest carbon estimation, using the 'percentage of the total points' reduction algorithm developed at Boise Center Aerospace Laboratory (BCAL LiDAR Tools, Idaho, USA). A total of eight models were developed to link field-measured AGB with LiDAR-derived variables at the four densities for deciduous and coniferous trees, respectively. Because those models were available from one of our previous research (see details in Singh et al., 2015a), they were directly used in the current study. (ii) LiDAR models developed at each point density were combined with the four NAIP classification maps to generate wall-to-wall deciduous/coniferous AGB estimates for the entire study area. This was followed by AGB conversion to aboveground carbon by multiplying a constant 0.5, a standard conversion factor used in many natural and urban forest studies (Hudak et al., 2012; McPherson et al., 2013; Myneni et al., 2001). Because all the LiDAR models were developed at the scale of 0.04 ha (400 m^2), the NAIP classification maps were resampled to the same scale (20 × 20 m grids) using the simple majority rule to define the final land-cover class for each grid. In total, we generated 16 carbon maps (four point densities of LiDAR point clouds × four resolutions of NAIP images) for the study area.

4.3. Extraction of landscape patterns

The spatial structure and patterns of urban neighborhoods can be quantified in a variety of ways. In this study, we followed the widely used *landscape metrics* (McGarigal et al., 2002) to evaluate five aspects of spatial patterns that may cause uncertainties in forest carbon estimation. Specifically, we calculated percentage of landscape area (PLAND), mean patch size (MPS), edge density (ED), contagion index (CONTAG), Shannon's diversity index (SHDI), and patch cohesion index (COHESION) to represent area (PLAND and MPS), shape complexity (ED), dispersion/interspersion (CONTAG), diversity (SHDI), and connectivity (COHESION) of landscape patches for the used neighborhoods. Refer to McGarigal et al. (2002) for detailed interpretations of each metric. In our study, the area metrics (i.e., PLAND and MPS) were derived from individual land-cover classes, while the other ones were extracted considering all the classes together. As suggested by Godwin et al. (2015), the majority of those five types of metrics demonstrated different value ranges across the four categories of Charlotte's residential neighborhoods with built-up densities from low, medium-low, medium-high, to high. Here, we anticipated that such cross-neighborhood variations in the metrics may cause uncertainties in urban forest carbon estimation, which was jointly affected by the choice of remote sensing resolution.

4.4. Analyses of uncertainties in forest carbon estimation

We evaluated two main factors causing uncertainties in forest carbon estimation, including (i) the resolution of remote sensing data (i.e., NAIP pixel size and LiDAR point density), and (ii) the spatial patterns of urban residential neighborhoods. Specifically, (i) we calculated neighborhood-level carbon variation (standard deviation) for two scenarios. First, we fixed the resolution of NAIP image, and extracted carbon variation by comparing four carbon maps that applied NAIP image of a chosen resolution and LiDAR data of all the four point densities. We repeated the process for all the four resolutions of NAIP images, respectively, and derived four forest carbon variation maps. All the variation values were averaged at the neighborhood level. Second, the entire process was similar as that in scenario one. Another four carbon variation maps were generated. However, the roles of NAIP and LiDAR were switched. Through scenario one, we intended to quantify the impact of changing LiDAR point density on carbon estimation; while scenario two emphasized on the analysis of changing NAIP image resolution. Finally, we generated eight neighborhood-level carbon variation maps. (ii) To further understand which aspects of urban spatial patterns have significantly contributed to such variation in remote sensing carbon estimation, we developed eight linear regression models to link the extracted landscape metrics (predictor variables; Section 4.3) with each of the eight neighborhood-level carbon variation values (response variable). Variance inflation factor (VIF) was calculated to avoid multicollinearity among the predictor variables. By following a common rule of thumb, the predictor variables were selected where VIFs were smaller than five in the final models. All the models were developed at a 0.05 significance level using Akaike's information criterion (AIC) for determining the best ones, with adjusted R^2 and RMSEs (root-mean-square errors) reported.

5. Results and discussion

5.1. Uncertainties in land-cover mapping

The overall accuracies for the study area's land cover mapping were 88.67%, 82.00%, 81.67%, and 83.67%, using NAIP at 1, 5, 10 and

20 m resolutions, respectively (Fig. 2; Tables 1–4). Obviously, the highest resolution of 1 m offered the most detailed information of the complex urban landscape, facilitating an accurate extraction of land cover. The other three resolutions of data had comparative performance, which was 5–7% inferior than that using the 1 m image. In all cases, both the user's and producer's accuracies for mapping forests (i.e., deciduous and coniferous trees) were consistently higher than 80%. Because of the distinct spectral

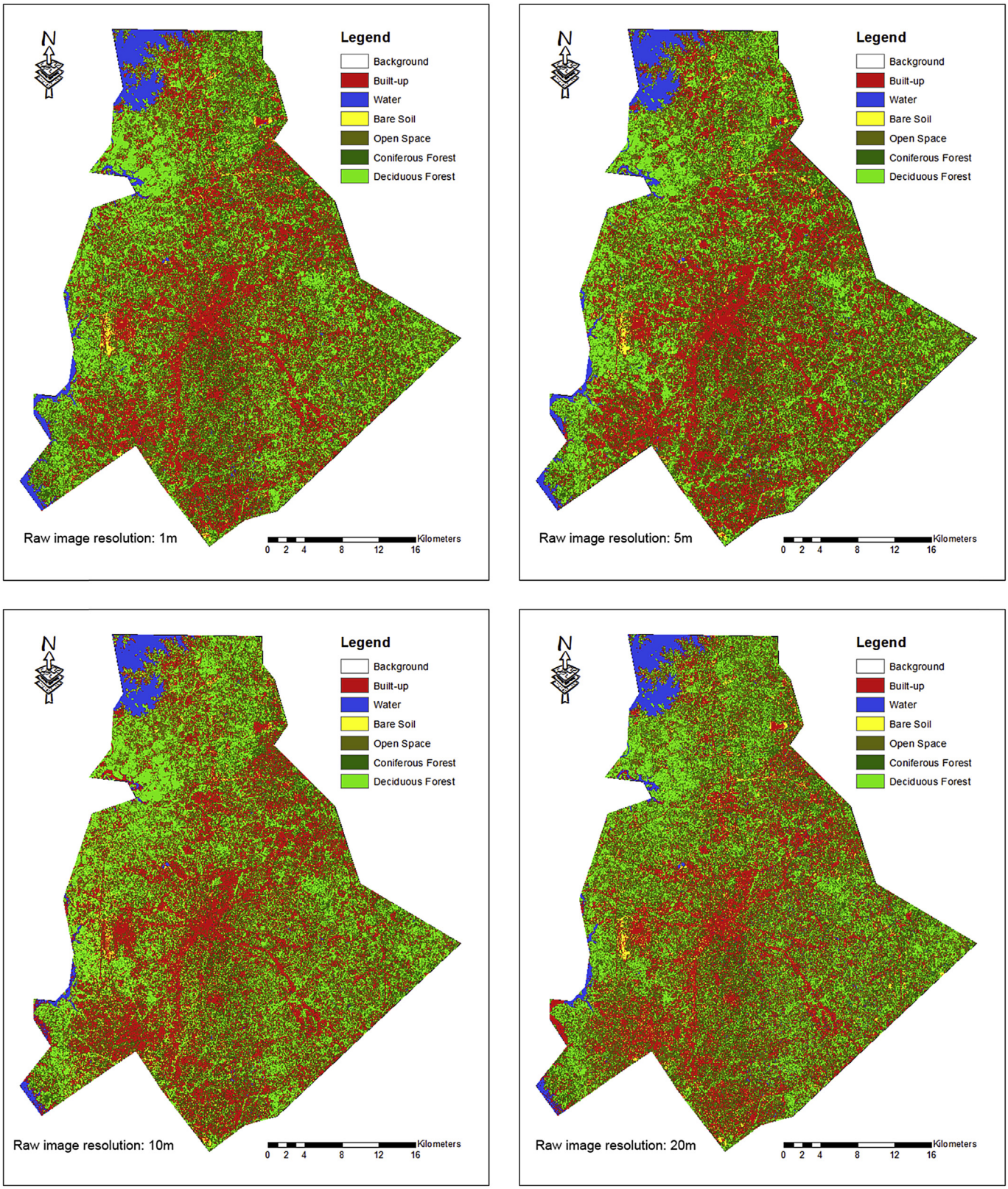

Fig. 2. Land-cover classification maps derived from four NAIP images with spatial resolutions of 1, 5, 10 and 20 m, respectively.

Table 1
Confusion matrix of the object-based image classification with 1 m NAIP image.

User class	Reference class							
	Bare soil	Built-up	Coniferous	Deciduous	Open space	Water	Total	User's accuracy (%)
Bare soil	14	2	0	0	1	0	17	82.35
Built-up	1	89	2	0	1	0	93	95.70
Coniferous	0	0	46	5	0	0	51	90.20
Deciduous	0	0	3	40	0	0	43	93.02
Open space	1	2	0	2	55	0	60	91.67
Water	0	10	4	0	0	22	36	61.11
Total	16	103	55	47	57	22	300	
Producer's accuracy (%)	87.50	86.41	83.64	85.11	96.49	100.00		

Overall accuracy = 88.67%; Kappa statistic = 0.86.

Table 2
Confusion matrix of the object-based image classification with 5 m NAIP image.

User class	Reference class							
	Bare soil	Built-up	Coniferous	Deciduous	Open space	Water	Total	User's accuracy (%)
Bare soil	14	1	0	0	2	0	17	82.35
Built-up	5	80	5	0	3	0	93	86.02
Coniferous	0	4	43	4	0	0	51	84.31
Deciduous	0	2	4	35	2	0	43	81.40
Open space	0	4	0	3	52	1	60	86.67
Water	0	13	1	0	0	22	36	61.11
Total	19	104	53	42	59	23	300	
Producer's accuracy (%)	73.68	76.92	81.13	83.33	88.14	95.65		

Overall accuracy = 82.00%; Kappa statistic = 0.77.

Table 3
Confusion matrix of the pixel-based image classification using 10 m NAIP image.

User class	Reference class							
	Bare soil	Built-up	Coniferous	Deciduous	Open space	Water	Total	User's accuracy (%)
Bare soil	10	7	0	0	0	0	17	58.82
Built-up	0	86	0	0	7	0	93	92.47
Coniferous	0	0	50	0	1	0	51	98.04
Deciduous	0	0	1	40	2	0	43	93.02
Open space	5	11	0	0	43	1	60	71.67
Water	0	20	0	0	0	16	36	44.44
Total	15	124	51	40	53	17	300	
Producer's accuracy (%)	66.67	69.35	98.04	100.00	81.13	94.12		

Overall accuracy = 81.67%; Kappa statistic = 0.76.

characteristics from vegetation as compared to other land-cover types, urban forests as a whole actually achieved an even higher accuracy. The major challenge was to accurately differentiating the deciduous from the coniferous trees. Coniferous trees typically look brighter in the near-infrared, red and green band combination due to the higher spectral reflectance in the near-infrared spectral range, which was captured by NAIP. However, the difference in spectral characteristics was difficult to be determined in some geographic areas covered by forests of mixed species types. This introduced uncertainties in the succeeding carbon estimation, because remote sensing carbon models were often developed for deciduous and coniferous tree, respectively, including the models used in our study.

While accuracy is an important criterion for assessing the

Table 4
Confusion matrix of the pixel-based image classification using 20 m NAIP image.

User class	Reference class							
	Bare soil	Built-up	Coniferous	Deciduous	Open space	Water	Total	User's accuracy (%)
Bare soil	14	2	0	0	1	0	17	82.35
Built-up	9	83	0	0	0	1	93	89.25
Coniferous	0	3	47	0	1	0	51	92.16
Deciduous	0	0	4	36	3	0	43	83.72
Open space	0	0	0	5	54	1	60	90.00
Water	0	19	0	0	0	17	36	47.22
Total	23	107	51	41	59	19	300	
Producer's accuracy (%)	60.87	77.57	92.16	87.80	91.53	89.47		

Overall accuracy = 83.67%; Kappa statistic = 0.79.

Fig. 3. Forest carbon maps derived from four resolutions (1, 5, 10 and 20 m) of NAIP images, four densities of LiDAR point clouds (100%, 80%, 40% and 20% of the original data).

mapping performance, it should be noted that image classification is typically calibrated and validated at specific scales using pixels or image-objects. Unlike their natural counterparts, urban landscapes are subject to a higher level of fragmentation. While a coarse resolution (e.g., 20 m) helped mitigate spectral noises caused by the variation in leaf reflection angles and the coexistence of sunlit and

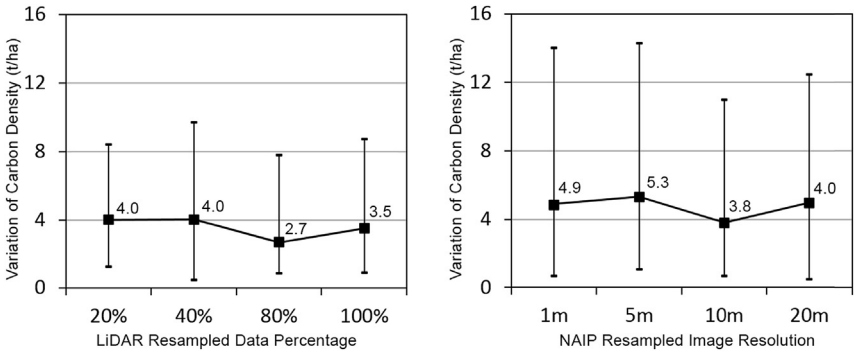

Fig. 4. Variation (standard deviation) of forest carbon density for using each of the four LiDAR point densities and each of the four NAIP image resolutions, respectively. The stock charts illustrate maximum, minimum, and average values.

shaded canopies, pixels tended to stride across landscape patches of different classes. Image-objects from a fine-resolution image (e.g., 5 m) were created with an intention to capture the actual geographic objects reducing the chances of comprising more than one type of land-cover patches in each object. Hence, the shapes of the basic study units for classifying coarse- and fine-resolution imagery were different (squared pixels *versus* image-objects of varying shapes). Although overall classification accuracies of land cover classifications were comparable, we observed inconsistencies on the edges of many landscape patches among those classified maps. The same reason may partially explain the variation in forest carbon estimates that used those baseline land-cover maps for determining forest spatial distribution.

5.2. Impacts of remote sensing resolution on forest carbon estimation

We generated a total of 16 forest carbon maps (Fig. 3) combing each of the four resolutions (1, 5, 10 and 20 m) of NAIP images, and each of the four densities of LiDAR point clouds (100%, 80%, 40% and 20%). While the spatial distributions of carbon showed similar patterns across the study area, the reduction of LiDAR point density noticeably reduced carbon estimates in many areas. This was especially true for small, isolated street trees, because low-density point clouds could have missed part of an individual tree (including canopy tops) and sometimes the entire canopies. However, in the relatively dense and large forest patches, the reduction of LiDAR point density affected carbon estimates marginally. This is because canopy structure of tree clusters was fairly captured by laser pulses (Singh et al., 2015a). The reduction of NAIP image resolution, however, affected carbon estimates in a different way. Such changes mainly occurred in two types of areas: on the edges between tree and non-tree patches, and within the mixed forest patches. As discussed in the previous section, different classification schemes (pixel-based *versus* object-based) were used to classify fine- and coarse-resolution NAIP images, causing inconsistent shapes and sizes of basic study units. On the edges of landscape patches, the estimation of carbon storage was observed to reveal higher variation than the areas not sitting on the edge of two or more types of land-cover patches.

We quantified carbon variation across the 50 tested neighborhoods following the analyses proposed in Section 4.4. When we fixed LiDAR point density and changed the resolution of NAIP image, the average carbon variation varied from 2.7 to 4.0 ha/t, corresponding to 6.2–8.6% of the average carbon densities derived from this study (Fig. 4). However, when we fixed NAIP resolution, the change of LiDAR point clouds introduced a higher variation in carbon estimation, from 3.8 to 5.3 t/ha, corresponding to 8.7–11.0% of the average carbon densities (Fig. 4). The results indicated that the change of remote sensing data resolution is likely to introduce noticeable uncertainties in urban forest carbon mapping. The difference in the range of variation further suggested a higher sensitivity of mapping accuracy to the choice of LiDAR point density than the optical image resolution.

5.3. Joint impacts of residential patterns and remote sensing resolution on forest carbon estimation

We developed eight linear regression models to explore the relationship between residential spatial patterns and the variation in remote sensing carbon estimates (see Section 5.2) at the neighborhood level (Table 5). The first four models were derived by fixing

Table 5
Linear regression models developed to link residential spatial patterns and forest carbon variation caused by the change of remote sensing data resolution.

Fixed data resolution	Equation	Adjusted R^2	RMSE(t/ha)
LiDAR 20%	$Y = -3.23^{*} + 0.08^{***} \times PLAND\_C3 - 0.50^{**} \times PLAND\_C6 + 3.48^{*} \times MPS\_C6 + 0.01^{***} \times ED$	0.44	1.32
LiDAR 40%	$Y = 3.37^{**} - 0.07^{***} \times PLAND\_C1 - 0.69^{***} \times PLAND\_C6 + 5.54^{**} \times MPS\_C6 + 0.01^{*} \times ED$	0.41	1.49
LiDAR 60%	$Y = -6.10^{**} - 0.18^{**} \times PLAND\_C2 - 0.08^{***} \times PLAND\_C3 - 0.59^{***} \times PLAND\_C6 + 2.41^{*} \times MPS\_C1 + 22.78^{**} \times MPS\_C2 + 5.00^{***} \times MPS\_C6 + 0.01^{***} \times ED$	0.50	0.98
LiDAR 100%	$Y = -1.03 - 0.10^{***} \times PLAND\_C1 - 0.24^{**} \times PLAND\_C2 - 0.53^{***} \times PLAND\_C6 + 3.04^{*} \times MPS\_C1 + 29.47^{**} \times MPS\_C2 + 4.28^{**} \times MPS\_C6 + 0.01^{***} \times ED$	0.55	1.13
NAIP 1 m	$Y = 444.03^{***} + 0.41^{***} \times PLAND\_C2 + 0.15^{***} \times PLAND\_C3 - 8.11^{***} \times MPS\_C3 + 33.18^{***} \times MPS\_C4 + 0.26^{**} \times CONTAG - 4.64^{***} \times COHESION$	0.78	1.33
NAIP 5 m	$Y = -1.40^{*} + 0.41^{***} \times PLAND\_C2 + 0.10^{***} \times PLAND\_C3$	0.76	1.34
NAIP 10 m	$Y = 308.69^{**} + 0.27^{***} \times PLAND\_C2 + 0.10^{***} \times PLAND\_C3 - 0.01^{**} \times ED - 3.09^{**} \times COHESION$	0.79	1.06
NAIP 20 m	$Y = 303.58^{***} + 0.29^{***} \times PLAND\_C2 + 0.12^{***} \times PLAND\_C3 - 3.07^{***} \times COHESION$	0.80	1.12

Level of significance: $^{*}p < 0.05$; $^{**}p < 0.01$; $^{***}p < 0.001$.
Y: neighborhood level carbon variation; *Ci*: Land-cover class *i* (C1: deciduous forest, C2: coniferous forest, C3: built-up, C4: open space, C5: water, and C6: bare soil); PLAND_*Ci*: percentage of landscape area for class *i*; MPS_*Ci*: mean patch size for class *i*; edge density (ED); dispersion/interspersion (CONTAG); connectivity (COHESION).

LiDAR point density, which allowed us to investigate the impact of changing NAIP resolution on carbon estimation. The last four models were developed to assess the impact of changing LiDAR point density on carbon mapping. Results showed that the variation caused by reducing LiDAR point density was better explained by neighborhood patterns, i.e., higher R^2 values, than that from reducing NAIP resolution. This suggests a possibly stronger association between urban spatial patterns and the uncertainties using LiDAR in carbon estimation.

The comparison of four models within each group revealed relatively similar results. For example, the carbon variation by changing NAIP resolution was mainly explained by the percentage (PLAND_C6) and mean patch size (MPS_C6) of bare soil, and edge density (ED), which demonstrated negative, positive, and positive contributions, respectively (Table 5). High PLAND_C6 values often occurred in new and/or poorly maintained neighborhoods with relatively high densities of anthropogenic disturbances. Because the built structures were often close to each other in those neighborhoods, forest coverage was low, isolated, and clustered as green belts or greenways. Changing NAIP resolution did not affect identifying trees at the edges. However, when MPS_C6 and ED values were high, the corresponding neighborhoods were often subject to a high level of vegetation disturbances and fragmentation. Complex forest edges may also have introduced high uncertainties in remote sensing carbon estimation. The carbon variation by changing LiDAR point density was mainly explained by the percentage of coniferous forests (PLAND_C2), built-ups (PLAND_C3), and the connectivity of land patches (COHESION), which demonstrated positive, positive, and negative contributions, respectively (Table 5). The small percentage of coniferous trees in the region was found to be heavily shaped by built objects, e.g., those planted in the yards as green fence. They showed a similar impact as built-ups, where a denser development pattern introduced a higher level of uncertainties in LiDAR-based carbon estimation. The negative impact of COHENSION indicated a strong impact of the subdivided nature of urban landscapes on forest carbon estimation from multiple densities of LiDAR data.

6. Conclusions

Spatially explicit measurement of forest vertical structure, e.g., carbon storage, in urban landscapes provides a crucial baseline map informing sustainable urban forest management. Our study investigated the impact of data resolution from aerial photography and small footprint LiDAR on forest carbon estimation. This was followed by quantifying how various types of neighborhood development patterns affected the accuracy-resolution tradeoff in a fast-growing, complex urban environment across the Charlotte-Mecklenburg County of North Carolina. Results indicated that the change of optical image resolution (from 1 to 20 m) and LiDAR point density (from 5.8 to 1.2 pt s/m^2) introduced noticeable uncertainties (variation) in forest carbon estimation at the neighborhood level. In our assessment, such uncertainties were more sensitive to changing LiDAR point density (causing 8.7–11.0% of variation at the neighborhood level) than changing optical image resolution (causing 6.2–8.6% of variation at the neighborhood level). We also found significant impacts of neighborhood spatial patterns on carbon variation by changing remote sensing data resolution. For both data types, a high level of anthropogenic disturbances (e.g., high percentage of built-up or high degree of tree patch fragmentation) introduced high variation in forest carbon estimation. While LiDAR-induced uncertainties were negatively affected by landscape patch connectivity, NAIP-induced variation was found to be positively correlated with the complexity of patch shape. In this research, we divided forests into two broad types of deciduous and coniferous trees. Although detailed species types were not extracted owing to sensor limitations, the study is one of the first evaluations quantifying uncertainties and their relationships with remote sensing data resolution and complex urban patterns. Although modeling fine-scale forest carbon storage could introduce errors, this study assessed uncertainties mainly at the neighborhood level. Because tree species types are generally not bound to certain neighborhoods, we believe that the errors associated with species did not have a major impact on our findings, which can therefore inform effective urban forest management in many other cities.

Acknowledgements

This research was supported by the North Carolina Space Grant, and the University of North Carolina at Charlotte CLAS Junior Faculty Development Award. Field date acquisition and processing were support by the National Science Foundation ULTRA-Ex program (BCS-0949170).

References

Alvey, A.A., 2006. Promoting and preserving biodiversity in the urban forest. Urban For. Urban Green. 5, 195–201.
American Forests, 2014. 10 Best Cities for Urban Forests. Retrieved from. http://www.americanforests.org/our-programs/urbanforests/10-best-cities-for-urban-forests.
BenDor, T., Shoemaker, D.A., Thill, J., Dorning, M.A., Meentemeyer, R.K., 2014. A mixed-methods analysis of social-ecological feedbacks between urbanization and forest persistence. Ecol. Soc. 19, 3.
Blaschke, T., Hay, G.J., Kelly, M., Lang, S., Hofmann, P., Addink, E., Raul, R.Q., van der Meer, F., van der Werff, H., van Coillie, F., Tiede, D., 2014. Geographic object-based image analysis – towards a new paradigm. ISPRS J. Photogramm. Remote Sens. 87, 180–191.
Census Bureau, 2015. 2014 State & County QuickFacts. Retrieved from. http://quickfacts.census.gov/qfd/states/37/37119.html.
Chen, G., Hay, G.J., St-Onge, B., 2012. A GEOBIA framework to estimate forest parameters from lidar transects, Quickbird imagery and machine learning: a case study in Quebec, Canada. Int. J. Appl. Earth Obs. Geoinform. 15, 28–37.
City of Baltimore, 2007. Baltimore City's Urban Forest Management Plan, 86p.
City of Charlotte, 2013. Urban Forestry Management Plan, 89p.
City of Charlotte and Mecklenburg County, 2012. Quality of Life Dashboard. Retrieved from. http://mcmap.org/qol/.
City of New York, 2014. Urban Forest Management Plans (For Eight Communities). Retrieved from. http://www.nycgovparks.org/trees.
City of Seattle, 2013. Urban Forest Stewardship Plan, 79p.
Clark, J.R., Matheny, N.P., Cross, G., Wake, V., 1997. A model of urban forest sustainability. J. Arboric. 23, 17–30.
Dwyer, J.F., Mcpherson, E.G., Schroeder, H.W., Rowntree, R.A., 1992. Assessing the benefits and costs of the urban forest. J. Arboric. 18, 227–234.
Godwin, C., Chen, G., Singh, K.K., 2015. The impact of urban residential development patterns on forest carbon density: an integration of LiDAR, aerial photography and field mensuration. Landsc. Urban Plan. 136, 97–109.
Hudak, A.T., Strand, E.K., Vierling, L.A., Byrne, J.C., Eitel, J.U.H., Martinuzzi, S., Falkowski, M., 2012. Quantifying aboveground forest carbon pools and fluxes from repeat LiDAR surveys. Remote Sens. Environ. 123, 25–40.
Jakubowski, M.K., Guo, Q.H., Kelly, M., 2013. Tradeoffs between lidar pulse density and forest measurement accuracy. Remote Sens. Environ. 130, 245–253.
Jenkins, J.C., Chojnacky, D.C., Heath, L.S., Birdsey, R.A., 2003. National-scale biomass estimators for United States tree species. For. Sci. 49, 12–35.
McGarigal, K., Cushman, S.A., Neel, M.C., Ene, E., 2002. FRAGSTATS: Spatial Pattern Analysis Program for Categorical Maps. University of Massachusetts, Amherst, MA.
McPherson, E.G., Xiao, Q., Aguaron, E., 2013. A new approach to quantify and map carbon stored, sequestered and emissions avoided by urban forests. Landsc. Urban Plan. 120, 70–84.
Myneni, R.B., Dong, J., Tucker, C.J., Kaufmann, R.K., Kauppi, P.E., Liski, J., Zhou, L., Alexeyev, V., Hughes, M.K., 2001. A large carbon sink in the woody biomass of Northern forests. Proc. Natl. Acad. Sci. U. S. A. 98, 14784–14789.
Nowak, D.J., Hirabayashi, S., Bodine, A., Hoehn, R., 2013. Modeled PM2.5 removal by trees in ten U.S. cities and associated health effects. Environ. Pollut. 178, 395–402.
Poudyal, N.C., Siry, J.P., Bowker, J.M., 2010. Urban forests' potential to supply marketable carbon emission offsets: a survey of municipal governments in the United States. For. Policy Econ. 12, 432–438.
Shrestha, R., Wynne, R.H., 2012. Estimating biophysical parameters of individual trees in an urban environment using small footprint discrete-return imaging lidar. Remote Sens. 4, 484–508.

Singh, K.K., Chen, G., Mccarter, J.B., Meentemeyer, R.K., 2015a. Effects of LiDAR point density and landscape context on estimates of urban forest biomass. ISPRS J. Photogramm. Remote Sens. 101, 310–322.
Singh, K.K., Davis, A.J., Meentemeyer, R.K., 2015b. Detecting understory plant invasion in urban forests using LiDAR. Int. J. Appl. Earth Observation Geoinform. 38, 267–279.
Treitz, P., Lim, K., Woods, M., Pitt, D., Nesbitt, D., Etheridge, D., 2012. LiDAR sampling density for forest resource inventories in Ontario, Canada. Remote Sens. 4, 830–848.
Tyrväinen, L., Miettinen, A., 2000. Property prices and urban forest amenities. J. Environ. Econ. Manag. 39, 205–223.
U.S. Department of Agriculture, 2015. NAIP Imagery. Retrieved from. http://www.fsa.usda.gov/programs-and-services/aerial-photography/imagery-programs/naip-imagery/.
Wear, D.N., Turner, M.G., Naiman, R.J., 1998. Land cover along an urban-rural gradient: implications for water quality. Ecol. Appl. 8, 619–630.